Iğdır Üniversitesi Fen Bilimleri Enstitüsü Dergisi, 16(3), 856-869, 2026
Journal of the Institute of Science and Technology, 16(3), 856-869, 2026

ISSN: 2146-0574, eISSN: 2536-4618

Bilgisayar Mühendisliği / *Computer Engineering* **DOI: 10.21597/jist.1957505**

Araştırma Makalesi / *Research Article*

Geliş tarihi / *Received*: 22.06.2026 **Kabul tarihi / *Accepted*: 22.07.2026**

Atıf İçin: Keles, A., Yasar, G. S., Algin, O., Farooqui, A. A. ve Akdemir Ozisik, P. (2026). PC-MRG'de Biyolojik Sıvı Akış Dinamiği Kullanılarak Ekstraventriküler Beyin Bölgelerinin Denetimsiz Segmentasyonu. *Iğdır Üniversitesi Fen Bilimleri Enstitüsü Dergisi*, 16(3), 856-869.

To Cite: Keles, A., Yasar, G. S., Algin, O., Farooqui, A. A. & Akdemir Ozisik, P. (2026). Unsupervised Segmentation of Extraventricular Brain Regions in PC-MRI Using CSF Flow Dynamics. *Journal of the Institute of Science and Technology*, 16(3), 856-869.

PC-MRG'de Biyolojik Sıvı Akış Dinamiği Kullanılarak Ekstraventriküler Beyin Bölgelerinin Denetimsiz Segmentasyonu

Ayse KELES[1,2], Gurkan Sinan YASAR[3], Oktay ALGİN[3,4], Ausaf A FAROOQUI[3], Pinar AKDEMİR OZİSİK[3]

Öne Çıkanlar:
- Beyin Omurilik Sıvısı Akış Dinamikleri
- Ekstraventriküler Beyin Bölgesi Analizi
- Perivasküler Akış Paternleri

Anahtar Kelimeler:
- PC-MRI
- Beyin Omurilik Sıvısı
- Gözetimsiz Segmentasyon
- K-means Kümeleme
- Ekstraventriküler Nörogörüntüleme
- Dalgacık Analiz

ÖZET:

Beyin Omurilik Sıvısı (BOS), sağlığın sürdürülmesinde kritik bir rol oynamaktadır; başta kardiyak döngü ve solunum tarafından yönlendirilen bu sıvının pulsatil hareketi değerli bir fizyolojik sinyal niteliği taşımakta olup anormallikleri giderek artan biçimde nörolojik bozukluklarla ilişkilendirilmektedir. Faz-kontrast manyetik rezonans görüntüleme (PC-MRG), hem anatomik yapıyı hem de akış özelliklerini non-invaziv biçimde yakalamaya olanak tanımaktadır. Bu çalışmada, ön komissür–arka komissür (AK–PK) hattı boyunca elde edilen PC-MRG verilerinden türetilen BOS akış dinamiklerini kullanarak ekstraventrikler beyin bölgelerini bölütlemeye yönelik denetimsiz bir yöntem önerilmektedir. PC-MRG verileri, kardiyak döngü başına 23–30 görüntü olacak şekilde sekiz sağlıklı gönüllüden (VENC = 10 cm/s) toplanmıştır. Zaman, frekans ve dalgacık (wavelet) domenlerinden elde edilen gösterimlerden çıkarılan voksel bazlı özellikler K-ortalamalar algoritması ile kümelenmiştir. Ablasyon çalışması, frekans domenine ait özelliklerin en ayrıştırıcı domain olduğunu doğrulamıştır. Uzman nöroradyologlar tarafından doğrulanan segmentler, ventrikül ötesindeki anatomik bölgelerle — gri madde, beyaz madde, vasküler yapılar ve BOS boşlukları — güçlü bir uyum sergilemiştir. Ayrıca segmente edilen bölgelerdeki BOS akış özellikleri de karşılaştırmalı analiz amacıyla incelenmiş ve sunulmuştur. Ekstraventrikler bölgelere odaklanılarak tüm beyin genelinde BOS dinamiklerinin daha kapsamlı biçimde incelenmesi mümkün kılınmış; BOS'un çevre dokularla nasıl etkileşime girdiğine dair yeni bulgular ortaya konmuştur. Beyin genelinde uygulanan bu etiket-bağımsız yaklaşım, BOS akışının bozulduğu nörolojik durumların daha erken tespitine ve daha etkin izlenmesine zemin hazırlamakta; glimatik taşıma, nöroinflamasyon ve sıvı-doku etkileşimlerinin rolüne yönelik gelecekteki araştırmalar için temel oluşturmaktadır.

Unsupervised Segmentation of Extraventricular Brain Regions in PC-MRI Using CSF Flow Dynamics

Highlights:
- CSF Flow Dynamics
- Extraventricular Brain Region Analysis
- Perivascular Flow Patterns

Keywords:
- PC-MRI
- Cerebrospinal fluid
- Unsupervised segmentation
- K-means clustering
- Extraventricular neuroimaging
- Wavelet analysis

ABSTRACT:

Cerebrospinal fluid (CSF) plays a crucial role in maintaining health, and its pulsatile movement driven primarily by the cardiac cycle and respiration serves as a valuable physiological signal, with abnormalities increasingly associated with neurological disorders. Phase-contrast magnetic resonance imaging (PC-MRI) offers a non-invasive means of capturing both anatomical structure and flow characteristics. In this study, we propose an unsupervised method to segment extraventricular brain regions using CSF flow dynamics derived from PC-MRI data acquired along the anterior commissure–posterior commissure (AC–PC) line. PC-MRI data were collected from eight healthy volunteers (VENC = 10 cm/s) with 23–30 images per cardiac cycle. Voxel-wise features — extracted from time-, frequency-, and wavelet-domain representations —were clustered using the K-means algorithm. An ablation study confirmed that frequency-domain features are the most discriminative single domain. The resulting segments, validated by expert neuroradiologists, showed strong alignment with anatomical regions- grey matter, white matter, vasculature, and CSF spaces- beyond the ventricles. Additionally, the CSF flow characteristics within the segmented regions were also examined and presented for comparative analysis. By focusing on extraventricular regions, this method enables a more comprehensive analysis of CSF dynamics across the entire brain, offering new insights into how CSF interacts with surrounding tissues. This brain-wide, label-free approach opens the door to earlier detection and improved monitoring of neurological conditions where CSF flow is disrupted and lays the groundwork for future research into the role of glymphatic transport, neuroinflammation, and fluid-tissue interactions in both health and disease.

[1,2*]Ayse KELES (**Orcid ID:** 0000-0001-8760-412X), [1] University of Galway, School of Computer Science, Galway, Ireland, [2] Ankara Medipol University, Faculty of Engineering and Natural Sciences, Ankara, Türkiye
[3] Gurkan Sinan YASAR (**Orcid ID**:0000-0002-5513-630), Ausaf A FAROOQUI, (**Orcid ID**:0000-0001-8777-6298), Pinar AKDEMİR OZİSİK, (**Orcid ID**:0000-0001-5183-8100), National MR Research Center (UMRAM), Bilkent University, Ankara, Türkiye
[4,5] Oktay ALGİN, (**Orcid ID:**0000-0002-3877-8366), [4] Interventional MR Clinical R&D Institute, Ankara University, Ankara, Türkiye. [5] Radiology Department, Medical Faculty, Ankara University, Ankara, Türkiye

***Sorumlu Yazar/*Corresponding Author**: Ayse KELES, e-mail: ayse.keles@universityofgalway.ie

Etik Kurul Onayı / *Ethics Committee Approval*: Bu çalışma için Bilkent Üniversitesi İnsan Araştırmaları Etik Kurulu'ndan etik onay alınmış olup, görüntüleme işlemi öncesinde tüm katılımcılardan yazılı bilgilendirilmiş onam alınmıştır.

INTRODUCTION

In the context of Magnetic Resonance Imaging (MRI), Phase-contrast MRI (PC-MRI) with peripheral cardiac gating has emerged as a powerful non-invasive imaging modality for the qualitative and quantitative assessment of cerebrospinal fluid (CSF) and blood flow dynamics (Kim et al., 1999; Korbecki et al., 2019). By capturing velocity-encoded data synchronized with the cardiac cycle, PC-MRI provides detailed insights into pulsatile flow characteristics and temporal variations in intracranial and spinal fluid motion. The growing application of PC-MRI in neuroimaging has significantly enhanced our understanding of CSF physiology and contributed to the identification of pathological flow alterations in various neurological disorders (Menick, 2001; Battal et al., 2011; Kartal & Algin, 2014; Patel et al., 2018; Karki et al., 2025). Notably, CSF flow analysis via PC-MRI plays a crucial role in measuring key hemodynamic parameters to enable the investigation of pulsatility-related phenomena. Furthermore, PC-MRI data are increasingly used in conjunction with complementary physiological measurements to support comprehensive evaluations of CSF dynamics. For instance, Lokossou et al. successfully integrated PC-MRI-derived CSF flow parameters with intracranial pressure (ICP) monitoring to enhance diagnostic accuracy and improve the interpretation of cerebrospinal hemodynamics (Lokossou et al., 2018).

Segmentation of brain and CSF components in MRI data using machine learning algorithms has been widely studied (Wu et al., 2025). While conventional MRI primarily provides anatomical insights, PC-MRI adds a crucial functional layer by capturing CSF flow Dynamics (Kim et al., 1999; Korbecki et al., 2019). This unique capability has shifted research interest toward the segmentation of CSF regions specifically within PC-MRI data.

To contextualise the novelty of the proposed method, Table 1 provides a structured comparison of published PC-MRI segmentation studies. As shown in the table, most previous studies on brain segmentation using PC-MRI data have primarily focused on the ventricular system, our study takes a novel approach by targeting the extraventricular regions intersected by the anterior commissure–posterior commissure (AC–PC) line. The AC–PC line, drawn horizontally from the superior surface of the anterior commissure to the posterior commissure in the sagittal plane (illustrated in Figure 2), serves as a fundamental anatomical reference in neuroimaging for standardizing brain orientation and positioning (Choi et al., 2013). Therefore, our work represents a significant step toward expanding CSF flow analysis beyond the ventricles and may contribute to future studies on CSF in the entire brain.

The existing methods—whether based on classical signal processing techniques or supervised DL—have predominantly focused on segmenting a single tissue class, most commonly CSF, within the ventricular system or cervical spinal canal. In contrast, no previous study has simultaneously segmented white matter, grey matter, CSF, and blood vessels in the extraventricular brain using an unsupervised learning framework applied to PC-MRI data. This gap in the literature highlights the novelty and contribution of the proposed approach. The segmentation was performed using the unsupervised K-means clustering algorithm (Oti et al., 2021), which enables tissue classification without requiring manual annotations. The algorithm partitions the dataset into a predefined number of clusters. In this study, four clusters—excluding the background—were defined to represent the distinct tissue types targeted for segmentation.

Conventional PC-MRI evaluations heavily rely on the manual delineation of anatomical regions, which introduces significant inter- and intra-observer variability and places a considerable burden on radiologists. By eliminating the dependency on manual input, the proposed unsupervised method

offers a more efficient, objective, and reproducible solution. Furthermore, this work aims to advance the evaluation of CSF distribution and dynamics within extraventricular brain regions, contributing to clinical research by demonstrating the potential of unsupervised machine learning techniques in facilitating scalable, high-precision analysis of functional MRI data.

Table 1. PC-MRI segmentation studies in the literature. WM = white matter; GM = grey matter; CSF = cerebrospinal fluid; BV = blood vessels; CA = cerebral aqueduct; SS = Silhouette Score; DBI = Davies–Bouldin Index; CHI = Calinski–Harabasz Index

Study	Region Targeted	Tissue(s) Segmented	Method	Learning Paradigm	Evaluation
Alperin & Lee (2003)	Cervical spinal canal	CSF + vascular lumen	PUBS (pulsatility-based threshold)	Unsupervised	Qualitative; flow volume
Sundareswaran et al. (2009)	Cardiovascular vessels	Blood flow lumen	Optimum fuzzy filters	Unsupervised	Velocity accuracy
Yoshida et al. (2009)	CA+Subarachnoid space	CSF	Correlation-coefficient analysis	Unsupervised	CSF flow rate
Stadlbauer et al. (2010)	Ventricular system	CSF flow patterns	MR velocity mapping	Unsupervised (rule-based)	Flow velocity maps
Abdullah et al. (2013)	Brain (ventricular)	CSF	Spatial fuzzy clustering + GMM	Unsupervised	Qualitative visual
Tsou et al. (2021)	CA only	CSF	2D U-Net (CNN)	Supervised	Dice, AUC, sensitivity
Keles et al. (2023)	Subarachnoid space	CSF	3D Attention U-Net	Supervised	Dice, IoU
Present Study	**Extraventricular brain (AC–PC line)**	**WM, GM, CSF, BV (4 classes)**	**K-Means + 19D engineered features**	**Unsupervised**	**SS, DBI, CHI + clinical expert review**

Secondly, motivation behind this work stems from the inherent limitations of phase images, which often lack sufficient spatial contrast to enable visual interpretation of anatomical features and CSF flow by clinicians. These images, although rich in hemodynamic information, are generally difficult to interpret using conventional means. To address this challenge, our approach incorporates pulsatile flow dynamics—representing fluid motion across the cardiac cycle—into the segmentation framework. By leveraging temporal variations in flow, our method enhances the interpretability of phase data and enables the extraction of clinically meaningful visual representations. This strategy has the potential to generate novel diagnostic insights and facilitate improved visualization of CSF dynamics, particularly within extraventricular brain regions, thereby broadening the clinical applicability of PC-MRI in neuroimaging contexts.

MATERIALS AND METHODS

The overall machine learning framework of the study consists of three main stages: dataset preparation, feature extraction, and clustering. Initially, raw PC-MRI DICOM datasets were preprocessed to enhance image quality and generate anatomically constrained brain masks. The second stage involves extracting a rich set of features from each voxel's temporal flow signal, capturing statistical, spectral, and wavelet-domain characteristics. Finally, in the clustering phase, the K-means algorithm is employed to group pixels based on their flow-related characteristics, enabling segmentation of functionally distinct regions without requiring manual annotations. Implementation flowchart is illustrated in Figure 1.

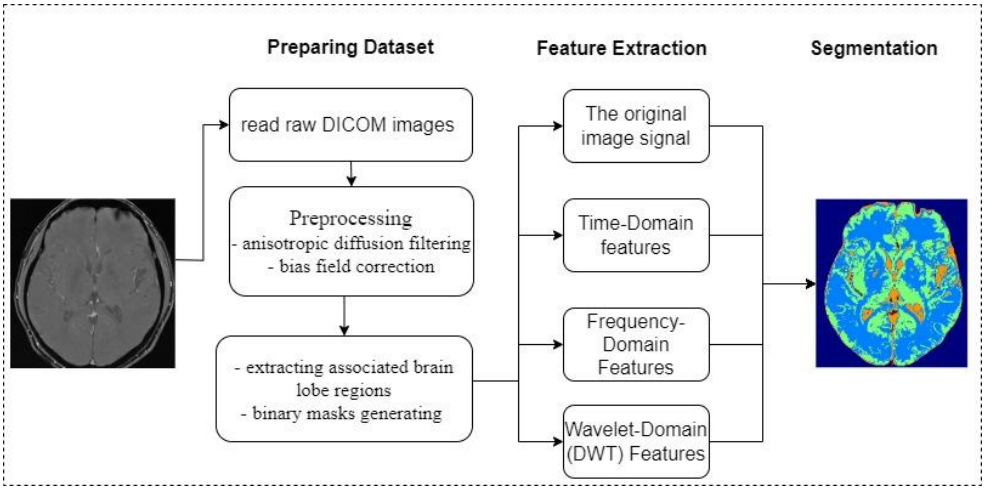

Figure 1. Overview of the proposed framework

Dataset

The PC-MRI dataset utilized in this study was acquired from eight healthy adult volunteers (four female, four male) using a Siemens 3T MRI scanner at the National Magnetic Resonance Research Center (UMRAM) in Ankara, Türkiye. Ethical approval was granted by Bilkent University Human Research Ethics Committee, and written informed consent was obtained from all participants prior to imaging. The participants had a mean age of 38 years. Axial images were acquired in alignment with the AC-PC plane, as illustrated in Figure 2. For each acquisition, both average modulus (rephase) images and directional phase difference (phase) images were obtained at corresponding spatial coordinates using peripheral cardiac gating. The imaging parameters were as follows: matrix size = 256 × 256, field of view (FOV) = 19 × 19 cm², repetition time (TR) = 29.25 ms, echo time (TE) = 7.03 ms, slice thickness = 3 mm, flip angle = 100°, and velocity encoding (VENC) = 10 cm/s. The number of phase images acquired in the cine loop varied depending on the subject's cardiac cycle. The temporal resolution of each patient images varies between 23 to 30. An example of rephase and phase images, along with their mean velocity matrices across the cine loop, is presented in Figure 3.

The method was implemented in PYTHON programming language with PyCharm Integrated Development Environment (IDE) and 64-bit Windows environment.

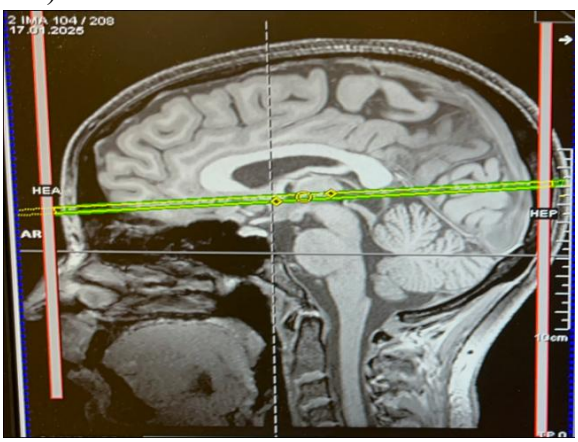

Figure 2. Anatomical reference of the axial imaging plane used in this study. The imaging was acquired at the level of the AC-PC line

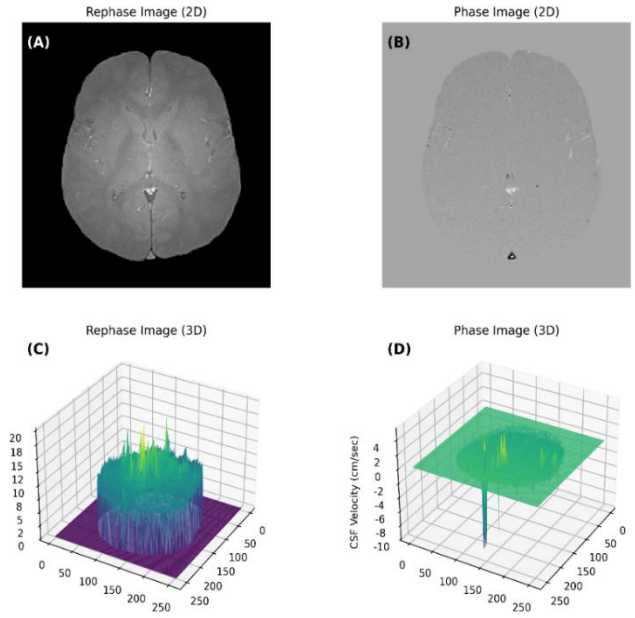

Figure 3. Spatial distribution and magnitude of CSF pulsatile flow dynamics: (A) and (B) show 2D brain-masked rephase and phase images, respectively, while (C) and (D) present corresponding 3D surface visualizations of mean CSF velocity matrices derived from temporal frames across the cardiac cycle

A- Preprocessing

In the preprocessing pipeline of this study, PC-MRI brain images were processed through a sequence of steps to enhance image quality and prepare the data for segmentation and clustering. Initially, raw DICOM images were read and stored data frame. Then rephase images subjected to anisotropic diffusion filtering (Weickert, 1998) to reduce noise while preserving edges. Subsequently, bias field correction was applied using the N4ITK python library to eliminate low-frequency intensity non-uniformities commonly present in MR images. To support anatomical alignment, binary masks were generated by extracting associated brain lobe regions removing the skull. These masks were later utilized to define and constrain the segmentation boundaries during the clustering process. The entire preprocessing and segmentation pipeline was implemented in Python (v3.11), utilizing open-source libraries such as NumPy, Pandas, tqdm, and scikit-learn for data manipulation, visualization, and machine learning.

B- Feature Extraction

The provided code implements a comprehensive feature extraction pipeline. This process specifically targets the pulsatile nature of CSF flow captured in PC-MRI data, which can be interpreted as time-resolved signals representing velocity variations across the cardiac cycle. By extracting voxel-wise signals from velocity-encoded phase images for each slab, the pipeline generates feature sets that encapsulate both spatial and temporal characteristics of CSF dynamics. After isolating the brain region on phase images using generated brain lobe mask in preprocessing step, each voxel's temporal signal—representing flow-related intensity variations over the cardiac cycle—is extracted. Summary of extracted features represented in Table 2.

The extracted features are concatenated with the original signal to form an augmented feature vector. These vectors are then standardized using z-score normalization with StandardScaler from Scikit-learn library. The resulting feature matrix serves as the input for the K-means clustering algorithm, which groups pixels into K tissue categories based on shared temporal and spectral flow characteristics. This feature extraction strategy is specifically tailored to exploit the pulsatile nature of CSF flow and aims to improve the discrimination of functionally distinct anatomical regions in the absence of manual annotations.

Table 2. Summary of extracted features: The table categorizes features into time-domain, frequency-domain, and wavelet-domain, providing each feature's name, mathematical formulation, and a brief explanation (x: signal vector, N: number of samples, μ,σ: mean and standard deviation of the signal, cA, cD: approximation and detail coefficients from Discrete Wavelet Transform (DWT), $P(\cdot)$: normalized power or probability distribution, ϵ: small constant to avoid log(0))

Feature Domain	Feature Name	Formula / Method	Explanation
Time-Domain	Mean	$\mu = \frac{1}{N}\sum_{i=1}^{N} x_i$	The average value of CSF flow throughout the cardiac cycle.
	Variance	$\sigma^2 = \frac{1}{N}\sum_{i=1}^{N}(x_i - \mu)^2$	CSF flow dispersion from the mean.
	Median	Middle value after sorting	Central value of CSF flow; less sensitive to flow outliers.
	Skewness	$\text{Skew}(x) = \frac{1}{N}\sum_{i=1}^{N}\left(\frac{x_i - \mu}{\sigma}\right)^3$	Indicates asymmetry of the signal distribution.
	Kurtosis	$\text{Kurt}(x) = \frac{1}{N}\sum_{i=1}^{N}\left(\frac{x_i - \mu}{\sigma}\right)^4$	Measures "tailedness" of the distribution.
	Signal Energy	$E = \sum_{i=1}^{N} {x_i}^2$	Total power or energy of the CSF flow signal.
	Slope	Linear fit slope of x vs. time	Trend of the CSF flow over cardiac cycle.
Frequency-Domain	Peak Frequency Index	$\text{argmax}\lvert\text{FFT}(x)\rvert$	Frequency bin with the highest magnitude (excluding DC).
	Peak Frequency Magnitude	$\max\lvert\text{FFT}(x)\rvert$	Magnitude of the dominant frequency component.
	Spectral Centroid	$\frac{\sum_i f_i P(f_i)}{\sum_i P(f_i)}$	Center of mass of the power spectrum.
	Spectral Entropy	$-\sum_i P(f_i)\log_2(P(f_i) + \varepsilon)$	Spectral complexity or randomness.
Wavelet-Domain (DWT)	Approximation Mean	$\text{mean}(cA)$	Average of low-frequency DWT coefficients.
	Approximation Variance	$\text{var}(cA)$	Dispersion in low-frequency components.
	Approximation Energy	$\sum_i {cA_i}^2$	Energy in the approximation coefficients.
	Approximation Entropy	$-\sum_i P({cA_i}^2)\log_2(P({cA_i}^2) + \varepsilon)$	Entropy in low-frequency approximation.
	Detail Mean	$\text{mean}(cD)$	Average of high-frequency DWT coefficients.
	Detail Variance	$\text{var}(cD)$	Dispersion in high-frequency components.
	Detail Energy	$\sum_i {cD_i}^2$	Energy in the detail coefficients.
	Detail Entropy	$-\sum_i P({cD_i}^2)\log_2(P({cD_i}^2) + \varepsilon)$	Entropy in high-frequency details.

All experiments were conducted on a standard laptop workstation equipped with a 13th Generation Intel® Core™ i7-1370P processor, 32 GB of DDR5 RAM. The pipeline consists of four sequential stages. Anisotropic diffusion filtering required approximately ~12 minutes total for the 8-subject dataset. N4 bias field correction was the most intensive step, requiring approximately 4.4 minutes per subject (total: ~35 minutes). Feature extraction and K-Means clustering (k=4) were in under one minute for the entire dataset, owing to the efficiency of scikit-learn's vectorized implementation. The computational profile of the method is therefore well within the capabilities of standard computing environments, and no cloud computing or high-performance cluster resources are necessary.

RESULTS AND DISCUSSION

Results

The PC-MRI images were segmented using the K-Means clustering algorithm with varying values of K. The elbow method is a widely adopted heuristic in mathematical optimization for identifying a cutoff point at which further increases in model complexity yield diminishing returns. In clustering, it is used to determine the optimal number of clusters by evaluating the balance between cluster compactness and model simplicity. The most common metric applied is the Sum of Squared Errors (SSE), which quantifies the total squared distance between each data point and the centroid of its assigned cluster. SSE is defined as follows:

$$SSE = \sum_{i=1}^{k} \sum_{x \in c_i} \|x - \mu_i\|^2 \quad (1)$$

where k is the number of clusters, C_i is the set of points in the i^{th} cluster, x is a data point, and μ_i is the centroid of the i^{th} cluster.

By plotting SSE as a function of the number of clusters, a curve is generated where the point of inflection—resembling an "elbow"—indicates the most suitable number of clusters. As illustrated in Figure 4, the elbow point, marked by a red circle, suggests that four clusters provide an optimal balance between accuracy and complexity for the given dataset.

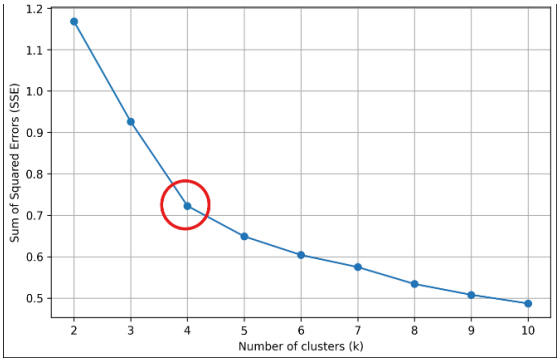

Figure 4. Elbow Method for Optimal K value. SSE as a function of the number of clusters

Expert evaluation of the resulting segmentations indicated a general consensus that K = 4 provides the most meaningful differentiation, successfully separating white matter, gray matter, CSF, and blood vessels. Figure 5 presents the segmentation outcomes for eight healthy volunteers, including the rephase, phase, brain-extracted, and clustered images. To provide a more in-depth understanding, one representative segmentation is examined in detail in Figure 6, where each tissue cluster is visualized independently. This detailed view enhances the interpretability of individual tissue classes and reinforces the anatomical validity of the segmentation. Clinical experts concurred that the clustering-based segmentations effectively delineated key anatomical structures, demonstrating the method's success in tissue differentiation. In this context, the segmented regions can be interpreted as representing (a) white matter, (b) gray matter, (c) cerebrospinal fluid, and (f) blood vessels.

Morover, the CSF flow characteristics within the segmented regions were also examined for comparative analysis. The boxplots Figure 7 presents the interquartile ranges of key flow metrics—namely, mean, peak, and median flow rates—across the segmented anatomical regions identified by the predictive model. The boxplot-based statistical evaluation of CSF dynamics across segmented brain tissues revealed significant variations in velocity characteristics among different regions. Notably, the CSF Regions exhibited the highest maximum intensities (mean = 5,48 cm/sec, SD = 0.67), substantially exceeding those of gray matter (mean = 4,35 cm/sec) and white matter (mean = 3,22 cm/sec). This elevated maximum flow is consistent with the physiological expectation that CSF, being a mobile fluid, demonstrates pulsatile movement patterns with greater peak velocities compared

to surrounding tissue structures. Interestingly, when examining mean and median velocity distributions, CSF regions exhibited negative values (mean =-0,69 cm/sec; median = -0,32 cm/sec), which may reflect retrograde flow phases due to the bidirectional pulsatility driven by cardiac and respiratory cycles. In contrast, parenchymal regions such as white and gray matter displayed much narrower distributions with lower absolute values, aligning with their relatively static nature. These findings underscore the importance of regional segmentation when quantifying CSF dynamics, particularly in phase-contrast MRI analysis, as pooling or ignoring anatomical context may obscure clinically relevant flow abnormalities.

Finally, to quantify the individual and combined contributions of each engineered feature domain to segmentation performance, a systematic ablation study was conducted across all eight subjects using seven feature configurations: (i–iii) each domain in isolation — statistical (7-d), frequency-domain (4-d), and wavelet (8-d); (iv–vi) all pairwise combinations; and (vii) the full engineered set (19-d). For each configuration, K-Means clustering (k = 4) was applied and evaluated using three internal validity indices: Silhouette Score (SS; higher is better), Davies–Bouldin Index (DBI; lower is better), and Calinski–Harabasz Index (CHI; higher is better), computed as means across all subjects. Among the single-domain feature sets, the frequency-domain group achieved the best performance across all three metrics ($SS = 0.4385 \pm 0.0544$, $DBI = 0.8541 \pm 0.1349$, $CHI = 32{,}010 \pm 9{,}938$), substantially outperforming both the statistical and wavelet subsets. Pairwise combinations did not consistently improve upon the single frequency-domain subset: the Stat + Freq (11-d) configuration ($SS = 0.2509 \pm 0.0672$) showed increased DBI relative to frequency features alone, suggesting that statistical features introduce scale heterogeneity that partially dilutes cluster separation. The full 19-dimensional engineered set yielded the lowest Silhouette Score ($SS = 0.2013 \pm 0.0314$) and highest DBI (1.5311 ± 0.1545) of all configurations, consistent with the curse-of-dimensionality effect in high-dimensional clustering. Results are summarised in Table 3.

Table 3. Ablation study results: mean ± standard deviation of internal cluster validity indices across eight subjects for seven engineered feature configurations (K-Means, k = 4). SS = Silhouette Score (higher ↑); DBI = Davies–Bouldin Index (lower ↓); CHI = Calinski–Harabasz Index (higher ↑). Best value per column shown in bold

Feature Set	SS (↑)	DBI (↓)	CHI (↑)
Statistical (7d)	0.2842 ± 0.0403	1.2442 ± 0.1452	16.164 ± 4.030
Frequency (4d)	**0.4385 ± 0.0544**	**0.8541 ± 0.1349**	**32.010 ± 9.938**
Wavelet (8d)	0.2281 ± 0.0394	1.4400 ± 0.1964	11.777 ± 3.484
Stat + Freq (11d)	0.2509 ± 0.0672	1.3808 ± 0.2456	14.888 ± 4.283
Stat + Wavelet (15d)	0.2132 ± 0.0365	1.5463 ± 0.1480	12.014 ± 2.827
Freq + Wavelet (12d)	0.2284 ± 0.0355	1.4193 ± 0.1249	12.647 ± 3.746
All Engineered (19d)	0.2013 ± 0.0314	1.5311 ± 0.1545	12.330 ± 3.120

Discussions

In this study, we explored PC-MRI, a specialized imaging modality that has garnered increasing attention for its ability to provide insights into CSF flow dynamics. PC-MRI data from eight participants were analyzed using an unsupervised machine learning approach based on the K-Means clustering algorithm. The K-Means algorithm was selected over alternative unsupervised methods for several problem-specific reasons. First, K-Means scales linearly with the number of observations, making it computationally tractable for our pixel-level feature matrix of approximately 160,000–210,000 observations. Second, the number of anatomically meaningful tissue classes in the brain (white matter, grey matter, CSF, vessels) is approximately known a priori, which aligns well with K-Means' requirement for a pre-specified K; the elbow method further validates this choice empirically. Third, the centroids learned by K-Means directly represent prototypical temporal-spectral flow signatures for each tissue class, providing biologically interpretable cluster profiles. Fourth, unlike Gaussian Mixture Models (GMM), K-Means makes no parametric distributional assumptions, which is

advantageous given the non-Gaussian nature of pulsatile flow signals. DBSCAN and hierarchical agglomerative clustering were also considered but are sensitive to density and distance thresholds that are difficult to tune reliably in high-dimensional (19-dimensional) feature spaces without ground-truth labels (Ikotun et al., 2023). The results presented in the previous section were evaluated and discussed by clinical experts, as detailed below.

Challenges in Grey Matter Segmentation; A recurring observation across multiple cases is the inconsistent segmentation of grey matter. While the model successfully identified many grey matter regions, it struggled with maintaining the expected continuous and uniform "mantle-like" appearance of the grey matter around the brain in limited cases. This suggests a limitation in distinguishing between grey matter and surrounding CSF or other adjacent structures, particularly at the grey-white matter junction. This is a known inherent limitation of PC-MRI techniques, which are not optimized for detailed grey-white matter differentiation.

Choroid Plexus and Vessel Segmentation; The segmentation of choroid plexus and other vascular structures showed varying degrees of success. In some instances, the choroid plexus was correctly identified and segmented as a vascular structure, aligning with its anatomical nature as a vascularized tissue. However, in other cases, especially for smaller or less prominent vessels, the model either missed them or misclassified them. The discussion highlighted that very small or faint vascular structures, particularly when their signal intensity is close to that of the surrounding tissue or CSF in PC-MRI, pose a significant challenge for accurate segmentation. The proposition to consider choroid plexus as part of the vascular segmentation to avoid over-complicating the current 4-segmentation scheme is a pragmatic approach, acknowledging its vascular nature.

Cerebrospinal Fluid (CSF) Segmentation; The segmentation CSF generally appears to be robust. The model successfully distinguished CSF within ventricles and around brain structures, even accounting for individual variations in CSF volume and distribution. In the regions adjacent to paranasal sinuses or in the presence of flow artifacts, CSF segmentation is poor compared to other cranial parts.

Artifacts and Limitations of PC-MRI; A key limitation of PC-MRI lies in the presence of artifacts often arise from inappropriate velocity encoding, slice/patient position, air in paranasal sinuses (susceptibility artifacts), or head motion. These factors can lead to misinterpretation in some cases, where air-related or motion-induced artifacts are mistakenly identified as CSF or other structures due to overlapping signal intensities or distortion of flow-related features, necessitating careful post-segmentation review. However, to ensure robustness in future applications across larger and more diverse populations, co-registering PC-MRI data with CT images acquired along the AC–PC line may further improve skull-stripping accuracy. CT-derived bone segmentation can serve as a precise reference to reduce misclassifications near the brain–skull boundary, as supported by the literature on spatial correction in flow-sensitive MRI modalities (Weltens et al., 2001).

Standard overlap-based metrics such as Dice coefficient, Jaccard index, or IoU were not calculated in this study due to technical and practical limitations of the PC-MRI modality. PC-MRI phase and rephase images provide limited tissue contrast, making it difficult to reliably distinguish grey matter, white matter, and small vascular structures for precise voxel-level annotation. Accurate labeling would require additional T1- or T2-weighted images; however, acquiring these introduces extra scan time and potential inter-scan head motion, which can prevent reliable spatial alignment and voxel-wise correspondence. Instead, validation was performed using three complementary approaches: (1) internal cluster quality using the SSE-based elbow method, (2) qualitative assessment by experienced clinicians evaluating anatomical plausibility and regional consistency, and (3)

physiological consistency of CSF velocity patterns, which aligned with known pulsatile dynamics. Future studies with co-registered T1/T2 acquisitions and motion correction will enable formal quantitative evaluation and more precise voxel-level ground truth analysis.

Comparison with DL Methods: A direct quantitative comparison with supervised DL segmentation approaches — such as U-Net, nnU-Net, or TransUNet — was not feasible in the present study, as DL-based methods require large annotated datasets for training, which do not currently exist for whole-brain PC-MRI segmentation along the AC–PC line. This study presents the first attempt at this specific task, and there are no established benchmarks or publicly available labelled datasets against which supervised methods could be fairly evaluated. For reference, DL-based segmentation of conventional T1/T2-weighted MRI typically achieves Dice scores of 0.85–0.95 for standard brain tissue classes when trained on large annotated corpora (e.g., FastSurfer, SynthSeg). Recent deep learning studies on MRI-based brain analysis (Bayram et al., 2025; Aslan & Özüpak, 2025) have demonstrated that supervised models can achieve excellent performance when trained on large, well-annotated datasets. However, such annotated corpora are currently unavailable for whole-brain PC-MRI segmentation along the AC–PC line. The proposed unsupervised approach is positioned as a necessary first step: it establishes feasibility without any labelled data, and the resulting cluster assignments could serve as pseudo-labels to bootstrap semi-supervised or self-supervised DL models in future work.

Dataset Set Limitations: Although the study cohort comprises eight healthy adult volunteers, the analytical scale is substantially larger: operating at the pixel level, the K-Means algorithm processes approximately 20,000–26,000 independent feature vectors per subject, placing the effective sample size in the range of 160,000–210,000 observations. The eight-subject design therefore constitutes a well-powered proof-of-concept for the proposed pipeline, and the authors acknowledge that future work should validate the learned cluster topology against a larger, diagnostically heterogeneous cohort to confirm clinical generalisability. Extension to clinical populations — including patients with normal pressure hydrocephalus, Alzheimer's disease, brain tumours, and traumatic brain injury — is identified as a critical next step for establishing clinical applicability. It should also be noted that in pathological cases, the number or nature of tissue classes may differ from those observed in healthy brains, potentially requiring re-calibration of the optimal K or incorporation of pathology-specific features into the clustering framework.

A significant finding in was that, although PC-MRI is not inherently designed for tissue segmentation, it could effectively differentiate white matter, grey matter, vascular structures, and CSF regions—even without the use of prior labels or anatomical atlases. This likely results from the distinct water content and tissue densities that manifest as subtle but measurable motion differences, especially during the cardiac cycle and respiratory movements. Our results suggest that solid brain tissues themselves undergo distinguishable motion patterns within the cranial cavity, which are detectable using PC-MRI.

In this study, we employed whole-brain PC-MRI segmentation to assess CSF flow characteristics. This approach offers a more comprehensive evaluation compared to region-specific techniques such as the ALPS (Analysis along the Perivascular Space) index, a diffusion tensor imaging (DTI)-based marker commonly used to assess glymphatic function (Kikuta et al., 2025). While ALPS provides insights limited to specific perivascular regions, PC-MRI allows for the global assessment of CSF dynamics by capturing both the velocity and direction of flow across the entire brain. This broader perspective is particularly valuable for investigating glymphatic transport mechanisms and

could enhance our understanding of conditions like Alzheimer's disease, ischemic or traumatic injuries, mitochondrial disorders, and demyelinating diseases.

These observations open new possibilities for the application of PC-MRI beyond flow measurement. For instance, the technique shows potential in differentiating tumor tissue from peritumoral or vasogenic edema—an area where conventional anatomical MRI often struggles. By capturing fine-grained alterations in tissue motion dynamics, PC-MRI may contribute to non-invasive assessments of tumor infiltration and edema characterization. In conclusion, PC-MRI emerges as a promising imaging modality for exploring brain fluid mechanics and neurovascular interactions. Future advancements should aim to integrate PC-MRI with advanced segmentation algorithms, multimodal imaging techniques, and dedicated motion analysis tools. Expanding its role from a flow analysis tool to a comprehensive diagnostic resource could significantly enhance clinical decision-making and research on neurodegenerative and cerebrovascular diseases.

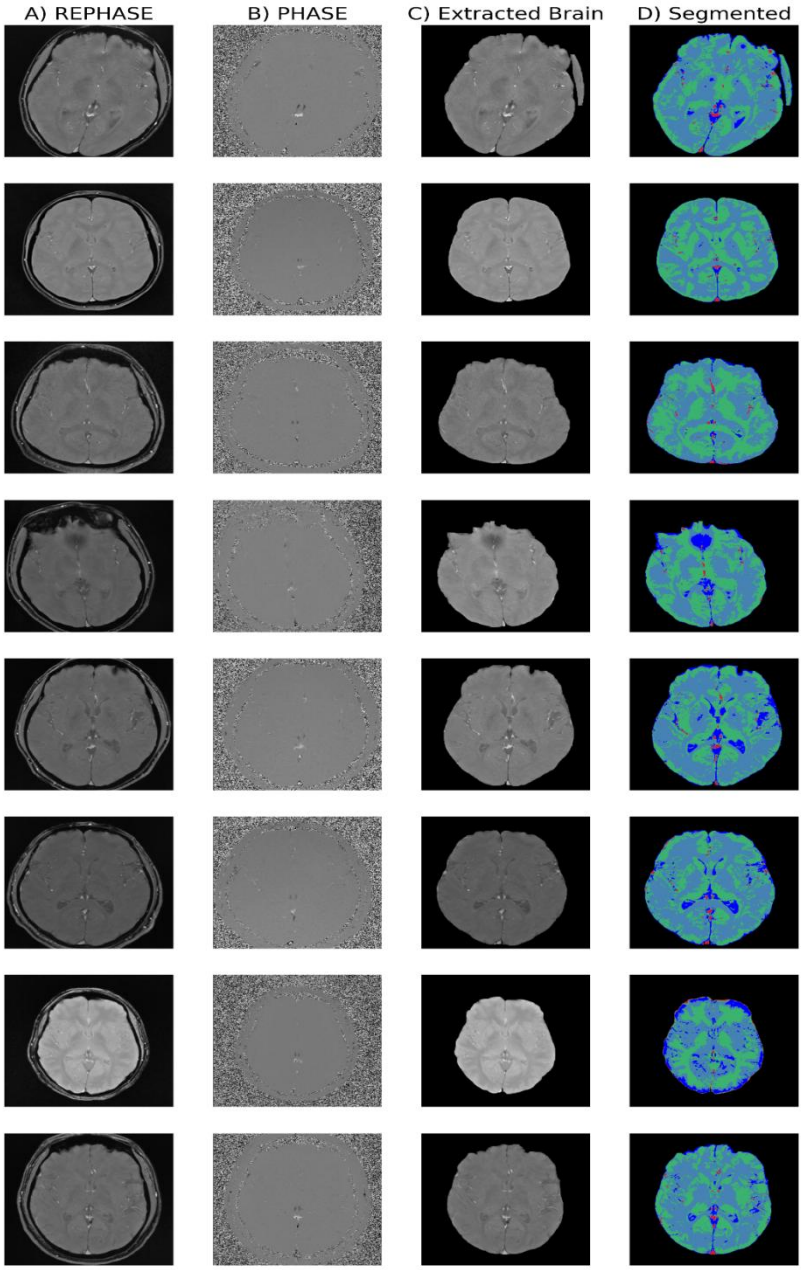

Figure 5. Segmentation results of PC-MRI images for eight healthy volunteers using K-Means clustering with K = 4. For each subject, four image types are displayed from left to right: the rephase image, the phase image, the brain-extracted image, and the final colour-coded segmented image. The segmentation differentiates four anatomical tissue types, each represented by a distinct colour: (a) white matter, (b) gray matter, (c) cerebrospinal fluid (CSF), and (d) blood vessels, as validated by expert neuroradiologist consensus

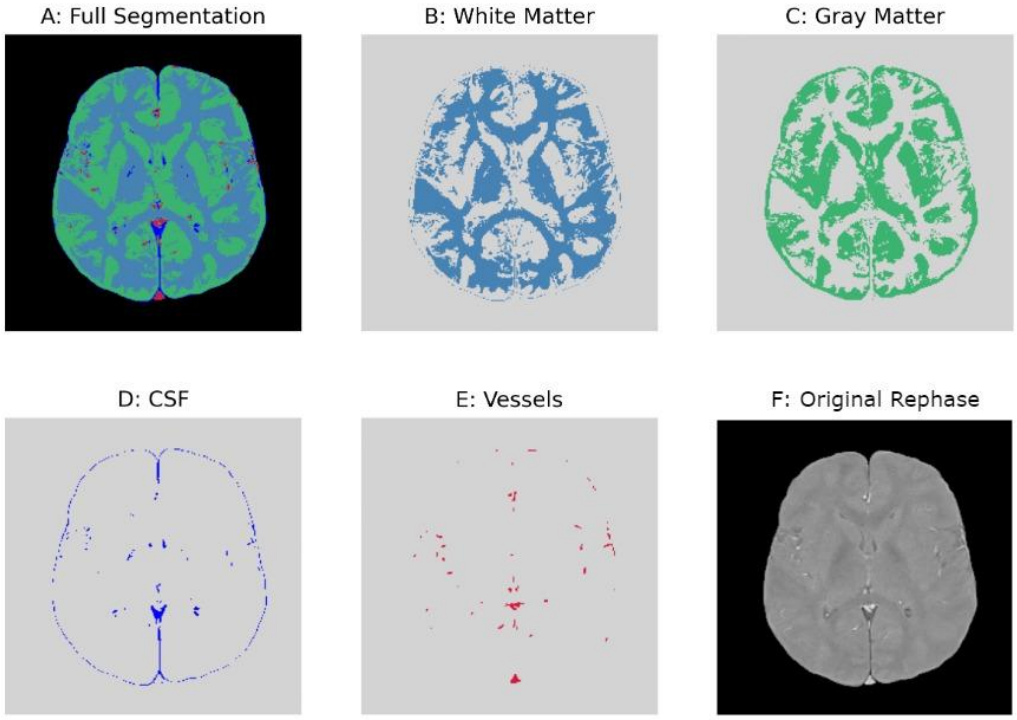

Figure 6. Detailed visualization of the segmented image from one representative subject. Each segmented regionis displayed individually to highlight the spatial distribution and structural differentiation

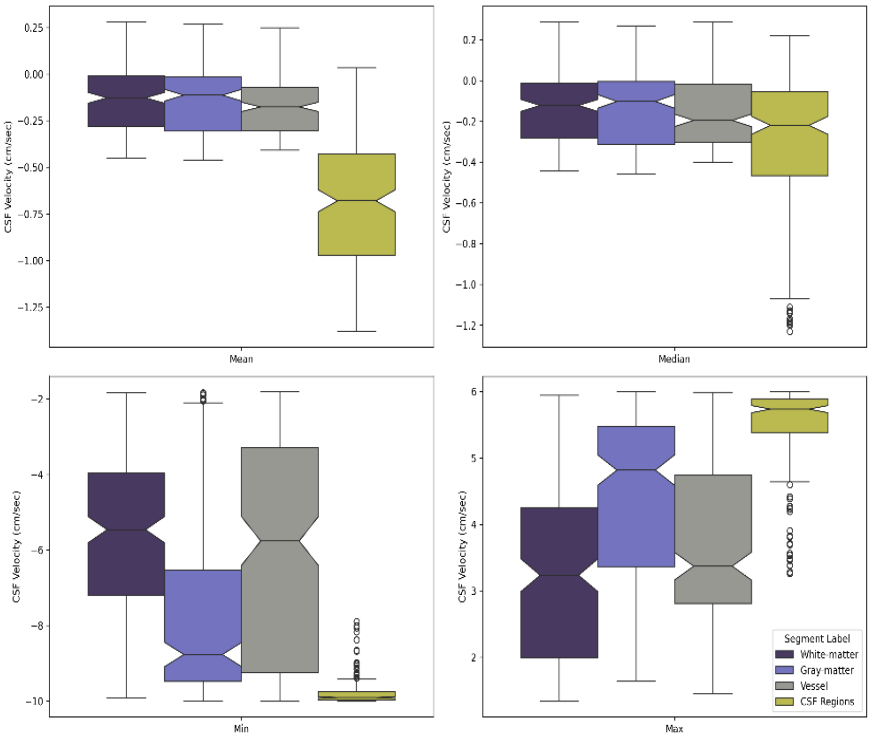

Figure 7. Comparison of CSF velocity statistics (Mean, Median, Min, Max) derived from the clustered brain segments. Each boxplot represents a specific segment (White Matter, Gray Matter, Vessel, and CSF Regions) across all subjects and time points. The y-axis represents CSF velocity in centimeters per second (cm/sec)

CONCLUSION

PC-MRI is a specialized imaging modality that enables the quantitative evaluation CSF flow by encoding velocity information into the MR signal—offering functional insights beyond conventional anatomical imaging. In this study, we applied an unsupervised k-means clustering algorithm to segment whole-brain PC-MRI data from eight healthy participants into four distinct tissue classes:

white matter, grey matter, vascular regions, and CSF. This segmentation was based on features derived from CSF flow dynamics, allowing us to classify brain tissues without prior labeling.

Notably, we present the first segmentation of extraventricular regions in PC-MRI images along the AC–PC line, marking a novel contribution to the literature. By extending PC-MRI analysis to the whole brain—particularly focusing on CSF evaluation beyond the ventricular system—it enables a more comprehensive and nuanced understanding of CSF dynamics and perivascular flow patterns.

Our findings highlight the untapped potential of PC-MRI for exploring neurofluid circulation and neurovascular coupling. Despite its limitations, PC-MRI demonstrated the capacity to distinguish between major brain tissues and visualize dynamic motion patterns, including subtle differences in tissue displacement. These capabilities suggest that PC-MRI could play an important role in the non-invasive assessment of conditions such as Alzheimer's disease, brain tumors, and ischemic injury, where alterations in CSF and vascular flow are clinically relevant.

Future research should focus on enhancing segmentation accuracy through advanced algorithms and integrating PC-MRI with multimodal imaging approaches. With further development, PC-MRI could become a valuable tool in both clinical diagnostics and neuroscience research for comprehensive evaluation of brain fluid mechanics.

Conflict of Interest

The article authors declare that there is no conflict of interest between them.

Author's Contributions

Conceptualization, A.K, P.A.O., and O.A.; Methodology, A.K., G.S.Y., O.A., and P.A.O.; Validation, O.A. and P.A.O; Investigation, A.K., A.A.F., and P.A.O.; Resources, A.K., O.A. and A.A.F.; Data Curation, A.K, G.S.Y., O.A., and P.A.O.; Writing—Original Draft, A.K and G.S.Y.; Writing—Review & Editing, A.K., G.S.Y., O.A., A.A.F. and P.A.O; Supervision, A.A.F. and P.A.O..

REFERENCES

Abdullah, A., Hirayama, A., Yatsushiro, S., Matsumae, M., & Kuroda, K. (2013). Cerebrospinal fluid image segmentation using spatial fuzzy clustering method with improved evolutionary expectation maximization. 2013 35th Annual International Conference of the IEEE Engineering in Medicine and Biology Society (EMBC),

Alperin, N., & Lee, S. H. (2003). PUBS: pulsatility-based segmentation of lumens conducting non-steady flow. Magnetic Resonance in Medicine: An Official Journal of the International Society for Magnetic Resonance in Medicine, 49(5), 934-944.

Aslan, E., & Özüpak, Y. (2025). Performance comparison of deep learning models in brain tumor classification. Balkan Journal of Electrical and Computer Engineering, 13(2), 203-209.

Battal, B., Kocaoglu, M., Bulakbasi, N., Husmen, G., Tuba Sanal, H., & Tayfun, C. (2011). Cerebrospinal fluid flow imaging by using phase-contrast MR technique. The British journal of radiology, 84(1004), 758-765.

Bayram, B., Kunduracioglu, I., İnce, S., & Pacal, I. (2025). A systematic review of deep learning in MRI-based cerebral vascular occlusion-based brain diseases. Neuroscience. https://doi.org/10.1016/j.neuroscience.2025.01.020

Choi, S.-H., Chi, J.-G., Kim, Y.-B., & Cho, Z.-H. (2013). Anterior commissure-posterior commissure revisited. Korean journal of radiology, 14(4), 653-661.

Ikotun, A. M., Ezugwu, A. E., Abualigah, L., Abuhaija, B., & Heming, J. (2023). K-means clustering algorithms: A comprehensive review, variants analysis, and advances in the era of big data. Information Sciences, 622, 178-210.

Karki, P., Murphy, M. C., Ganji, S., Gunter, J. L., Graff-Radford, J., Jones, D. T., Botha, H., Cutsforth-Gregory, J. K., Elder, B. D., & Jack Jr, C. R. (2025). Real-Time 2D Phase-Contrast MRI to Assess Cardiac-and Respiratory-Driven CSF Movement in Normal Pressure Hydrocephalus. Journal of Neuroimaging, 35(1), e70000.

Kartal, M. G., & Algin, O. (2014). Evaluation of hydrocephalus and other cerebrospinal fluid disorders with MRI: An update. Insights into imaging, 5, 531-541.

Keles, A., Algin, O., Ozisik, P. A., ŞEN, B., & Vehbi Çelebi, F. (2023). Segmentation of spinal subarachnoid lumen with 3D attention U-Net. Journal of Mechanics in Medicine and Biology, 23(04), 2340011.

Kikuta, J., Nagai, Y., Kamagata, K., Chen, H., Yamada, Y., Kitagawa, T., Uchida, W., Iseki, R., Guo, S., & Takabayashi, K. (2025). Association between frontal pole atrophy and glymphatic dysfunction in patients with bipolar disorder. Journal of Affective Disorders, 119686.

Kim, D.-S., Choi, J.-U., Huh, R., Yun, P.-H., & Kim, D.-I. (1999). Quantitative assessment of cerebrospinal fluid hydrodynamics using a phase-contrast cine MR image in hydrocephalus. Child's Nervous System, 15, 461-467.

Korbecki, A., Zimny, A., Podgórski, P., Sąsiadek, M., & Bladowska, J. (2019). Imaging of cerebrospinal fluid flow: fundamentals, techniques, and clinical applications of phase-contrast magnetic resonance imaging. Polish journal of radiology, 84, 240-250.

Lokossou, A., Balédent, O., Garnotel, S., Page, G., Balardy, L., Czosnyka, Z., Payoux, P., & Schmidt, E. (2018). ICP monitoring and phase-contrast MRI to investigate intracranial compliance. Intracranial Pressure & Neuromonitoring XVI,

Menick, B. J. (2001). Phase-contrast magnetic resonance imaging of cerebrospinal fluid flow in the evaluation of patients with Chiari I malformation. Neurosurgical Focus, 11(1), 1-4.

Oti, E. U., Olusola, M. O., Eze, F. C., & Enogwe, S. U. (2021). Comprehensive review of K-Means clustering algorithms. criterion, 12, 22-23.

Patel, R. P., Sitton, C. W., Ketonen, L. M., Hou, P., Johnson, J. M., Romo, S., Fletcher, S., Shah, M. N., Kerr, M., & Zaky, W. (2018). Phase-contrast cerebrospinal fluid flow magnetic resonance imaging in qualitative evaluation of patency of CSF flow pathways prior to infusion of chemotherapeutic and other agents into the fourth ventricle. Child's Nervous System, 34, 481-486.

Stadlbauer, A., Salomonowitz, E., Van Der Riet, W., Buchfelder, M., & Ganslandt, O. (2010). Insight into the patterns of cerebrospinal fluid flow in the human ventricular system using MR velocity mapping. Neuroimage, 51(1), 42-52.

Sundareswaran, K. S., Frakes, D. H., Fogel, M. A., Soerensen, D. D., Oshinski, J. N., & Yoganathan, A. P. (2009). Optimum fuzzy filters for phase-contrast magnetic resonance imaging segmentation. Journal of Magnetic Resonance Imaging: An Official Journal of the International Society for Magnetic Resonance in Medicine, 29(1), 155-165.

Tsou, C.-H., Cheng, Y.-C., Huang, C.-Y., Chen, J.-H., Chen, W.-H., Chai, J.-W., & Chen, C. C.-C. (2021). Using deep learning convolutional neural networks to automatically perform cerebral aqueduct CSF flow analysis. Journal of Clinical Neuroscience, 90, 60-67.

Weickert, J. (1998). Anisotropic diffusion in image processing (Vol. 1). Teubner Stuttgart.

Weltens, C., Menten, J., Feron, M., Bellon, E., Demaerel, P., Maes, F., Van den Bogaert, W., & van der Schueren, E. (2001). Interobserver variations in gross tumor volume delineation of brain tumors on computed tomography and impact of magnetic resonance imaging. Radiotherapy and Oncology, 60(1), 49-59.

Wu, L., Wang, S., Liu, J., Hou, L., Li, N., Su, F., Yang, X., Lu, W., Qiu, J., & Zhang, M. (2025). A survey of MRI-based brain tissue segmentation using deep learning. Complex & Intelligent Systems, 11(1), 1-16.

Yoshida, K., Takahashi, H., Saijo, M., Ueguchi, T., Tanaka, H., Fujita, N., & Murase, K. (2009). Phase-contrast MR studies of CSF flow rate in the cerebral aqueduct and cervical subarachnoid space with correlation-based segmentation. Magnetic Resonance in Medical Sciences, 8(3), 91-100.